The precipitation characteristics of ISCCP tropical weather states

by

Dongmin Lee[1,2,3], Lazaros Oreopoulos[2]

George J. Huffman[4,2], William B. Rossow[5], and In-Sik Kang[3]

1. GESTAR, University Space Research Association, Columbia, MD, USA

2. Earth Sciences Division, NASA-GSFC, Greenbelt, MD, USA

3. Seoul National University, Seoul, South Korea

4. Science Systems and Applications Inc., Lanham, MD

5. City College and Graduate School, City University of New York, New York, NY, USA

Submitted to the

Journal of Climate

December 2011

Corresponding author address:

Lazaros Oreopoulos

NASA-GSFC

Code 613

Greenbelt, MD 20771

USA

Lazaros.Oreopoulos@nasa.gov

Popular Summary

In order to understand the water budget of the planet it is important to measure the rainfall distribution. We can now achieve relatively good rainfall estimates from satellites over almost the entire planet. Only measuring rainfall amounts is however not enough for understanding the underlying physical processes that determine where, when, and how much rainfall occurs. We must also observe and measure other atmospheric characteristics that are related to rainfall, such as the properties of clouds. In this paper we propose a method that will help us better understand what cloud mixtures the precipitation of the tropical region (covering about half the are of the planet and exhibiting the strongest rainfall intensities) originates from. We achieve this by combining different satellite measurements targeted to rainfall and cloud thickness/height estimations. One of our main findings is that in the tropics about half of the total rainfall comes from one particular type of cloud mixtures, associated with deep storm systems. Surprisingly, our combined datasets indicate that even these clouds are often (about half the time) not precipitating (raining); when they do they tend to precipitate more strongly over ocean than over land, also a somewhat unexpected result given that several measures of storminess are stronger over land. Our results can be used to check whether climate models assign their precipitation in accordance with the observations and to therefore indirectly assess whether predictions of future precipitation in a changed climate are reliable.

Abstract

We examine the daytime precipitation characteristics of the International Satellite Cloud Climatology Project (ISCCP) weather states in the extended tropics (35°S to 35°N) for a 10-year period. Our main precipitation data set is the TRMM Multisatellite Precipitation Analysis 3B42 data set, but Global Precipitation Climatology Project daily data are also used for comparison. We find that the most convective weather state (WS1), despite an occurrence frequency below 10%, is the most dominant state with regard to surface precipitation, producing both the largest mean precipitation rates when present and the largest percent contribution to the total precipitation of the tropical zone of our study; yet, even this weather state appears to not precipitate about half the time. WS1 exhibits a modest annual cycle of domain-average precipitation rate, but notable seasonal shifts in its geographic distribution. The precipitation rates of the other weather states tend to be stronger when occuring before or after WS1. The relative contribution of the various weather states to total precipitation is different between ocean and land, with WS1 producing more intense precipitation on average over ocean than land. The results of this study, in addition to advancing our understanding of the current state of tropical precipitation, can serve as a higher order diagnostic test on whether it is distributed realistically among different weather states in atmospheric models.

The precipitation characteristics of ISCCP tropical weather states

by

Dongmin Lee[1,2,3], Lazaros Oreopoulos[2]

George J. Huffman[4,2], William B. Rossow[5], and In-Sik Kang[3]

1. GESTAR, University Space Research Association, Columbia, MD, USA

2. Earth Sciences Division, NASA-GSFC, Greenbelt, MD, USA

3. Seoul National University, Seoul, South Korea

4. Science Systems and Applications Inc., Lanham, MD

5. City College and Graduate School, City University of New York, New York, NY, USA

Submitted to the

Journal of Climate

December 2011

Corresponding author address:
Lazaros Oreopoulos
NASA-GSFC
Code 613
Greenbelt, MD 20771
USA
Lazaros.Oreopoulos@nasa.gov

Abstract

We examine the daytime precipitation characteristics of the International Satellite Cloud Climatology Project (ISCCP) weather states in the extended tropics (35°S to 35°N) for a 10-year period. Our main precipitation data set is the TRMM Multisatellite Precipitation Analysis 3B42 data set, but Global Precipitation Climatology Project daily data are also used for comparison. We find that the most convective weather state (WS1), despite an occurrence frequency below 10%, is the most dominant state with regard to surface precipitation, producing both the largest mean precipitation rates when present and the largest percent contribution to the total precipitation of the tropical zone of our study; yet, even this weather state appears to not precipitate about half the time. WS1 exhibits a modest annual cycle of domain-average precipitation rate, but notable seasonal shifts in its geographic distribution. The precipitation rates of the other weather states tend to be stronger when occuring before or after WS1. The relative contribution of the various weather states to total precipitation is different between ocean and land, with WS1 producing more intense precipitation on average over ocean than land. The results of this study, in addition to advancing our understanding of the current state of tropical precipitation, can serve as a higher order diagnostic test on whether it is distributed realistically among different weather states in atmospheric models.

1. Introduction

The role of clouds in the water and energy cycle can not be overstated. Atmospheric heating rates (due to radiative and thermodynamical processes), surface energy budgets (radiative and turbulent), and precipitation rates have strong dependencies on cloud properties, and frequency of occurrence. While the average effect of cloud can be studied in aggregate, grouping the multitude of observed cloud systems into discernible cloud regimes and studying the energy and water budgets associated with them can be a far more useful approach for understanding the potential impact of cloud changes on future water and energy budget distributions. An additional advantage of such a holistic approach is that more physically-based diagnostics to evaluate Global Climate Model (GCM) hydrological and radiative budgets can be formulated.

A number of recent studies have focused on the topic of objectively identifying distinct cloud regimes. The criterion commonly used for identifying cloud regimes is the co-variation of cloud location (expressed as cloud top height or pressure) and extinction (expressed as cloud optical thickness or reflectivity). Cloud mixtures exhibiting certain patterns in the co-variation of these quantities can be identified as distinct cloud regimes. The patterns can be identified with either neural network or *k*-means clustering techniques with the latter being generally easier to implement and therefore more popular (Jakob and Tselioudis 2003; Rossow et al. 2005; Zhang et al. 2007; Gordon and Norris 2010; Greenwald et al., 2010). The search for patterns can be performed on either a global dataset of joint height-extinction variations or on distinct climatic zones. The breakdown by climatic zone has the advantage that cloud regime identification can be fine-tuned so that cloud mixtures that may have otherwise been obscured in a larger data set can emerge from a more geographically targeted analysis. It also allows examing (dis)similarities between different parts of the globe with regard to the presence and occurence frequency of different cloud mixtures. Once the regimes have been identified, a variety of properties that characterize them can be easily compiled.

A compelling question is whether distinct roles of cloud regimes in weather and climate can be determined. If the atmospheric conditions under which particular cloud regimes form have indeed identifiable features, it should be possible to associate changes in meteorological conditions with changes in hydrology and energetics through these cloud regimes. Studies along such lines have begun to emerge in recent years. Several previous studies (Jakob et al. 2005; Williams and Webb 2008; Oreopoulos and Rossow 2011; Haynes et al. 2011) have focused on the radiative characteristics of cloud regimes. Other studies have concentrated on precipitation characteristics. For example, Jakob and Schumacher (2008) combined cloud regimes, inferred from International Satellite Cloud Climatology Project (ISCCP, Schiffer and Rossow 1983) cloud retrievals, with collocated precipitation and latent heating data from the Tropical Rainfall Measuring Mission (TRMM) Precipitation Radar in the tropical western Pacific. By compositing TRMM precipitation amount and type into the ISCCP regimes they managed to distinguish between three major precipitation regimes and identify their surface precipitation rates and latent heat profile characteristics. Zhang et al. (2010) defined cloud/precipitation regimes in the tropics from profiles of CloudSat/CALIPSO radar/lidar reflectivities and hydrometeor locations and then compared with the corresponding regimes of a GCM operating in weather forecast mode. Tromeur and Rossow (2008) found for the $\pm 15°$ latitude zone that while the most convectively active cloud regime dominated by organized deep convection dwarfs the precipitation rate of all other regimes, the regime representing unorganized convection with much lower average precipitation rate has nearly the same contribution, because it occurs much more frequently.

In this paper we conduct a more extensive and detailed analysis of the precipitation of tropical (±35° latitude zone) cloud regimes (henceforth referred to as "weather states" following Rossow et al. 2005 who explain that they are associated with distinct atmospheric conditions; see also Jakob and Tselioudis 2003; Jakob et al. 2005; Gordon and Norris 2010). One of our goals is to confirm that these mesoscale weather states as identified by ISCCP help in the understanding of tropical precipitation characteristics. Specifically, we examine the mean magnitude and range of surface precipitation rate produced by the weather states, their relative contribution to the total precipitation of the tropics, and the geographical distribution of weather state precipitation. We also seek to further clarify the degree to which the most convectively active weather states dominate the tropical precipitation, a topic also investigated by Rossow et al. (2011) with a different analysis approach. Our results are featured in section 4 which is broken into subsections, each highlighting separate important aspects of the precipitation-weather state relationship. We discuss means, geographical variations and frequency distributions of each weather state's precipitation rates, and dependencies on the precipitation data set used. We pay special attention to the strongest precipitating weather state, its seasonal variations and its apparent effects on the precipitation of the other weather states when in close temporal proximity.

2. Data sets

Our study uses three data sources: The ISCCP weather states for the extended tropics (Oreopoulos and Rossow 2011) to identify cloud regimes, and two precipitation products, the TMPA-3B42 (Huffman et al., 2010), and GPCP-1DD (Huffman et al., 2001).

Rossow et al. (2005) describe how the ISCCP weather state product is generated. Briefly, a search for distinctive patterns is conducted in the joint frequency distributions of cloud top pressure (p_c) and cloud optical thickness (τ) constructed from individual daytime satellite image pixel retrievals (fields-of-view about 5 km in size) within 2.5° regions provided in the International Satellite Cloud Climatology (ISCCP) D1 dataset (Rossow and Schiffer, 1999). Cluster centroids representing specific histogram patterns describing cloud variability are identified using the "*k*-means" clustering algorithm (Anderberg, 1973).

A weather state dataset derived as described above is now available for the period 1983-2008 between 65°S to 65°N divided in three geographical zones. This dataset can be downloaded from ftp://isccp.giss.nasa.gov/outgoing/PICKUP/CLUSTERS/data/1983-2008/. Here, we use the data corresponding to the so-called "extended" tropical/subtropical zone between 35°S and 35°N, ISCCP dataset D1.WS.ET.dat. This dataset has been previously used by Mekonnen and Rossow (2011) and Oreopoulos and Rossow (2011). The optimal cluster centroids are shown in Fig. 1, while maps of weather state relative frequency of occurrence (RFO) are provided in Fig. 2. The weather state indices were assigned according to classical understanding of associated convective activity strength, with indices increasing for the progressively more convectively suppressed weather states. Note that this indexing convention follows Rossow et al. (2005), but is opposite of that of Haynes et al. (2011).

The weather state data are jointly analyzed with two precipitation datasets for a 10-year overlapping period from January 1998 to December 2007. One is based on the Tropical Rainfall Measuring Mission (TRMM) Multi-satellite Precipitation Analysis (TMPA) algorithm which seeks to provide a "best" estimate of quasi-global (50°S to 50°N) precipitation from the wide variety of modern satellite-borne precipitation sensors as well as gauge measurements where feasible. Estimates are provided at relatively fine scales, 0.25°×0.25°, 3-hourly (Huffman et al. 2010). We use the post-processed research product which is based on calibration by the TRMM Combined Instrument (TCI) product and covers the period January 1998 to present. The research product system has been developed as the version 6 algorithm for the TRMM operational product 3B42 (3B42 V.6). Henceforth, we will call this product "TMPA-3B42".

The other precipitation product used is the GPCP-1DD version 1.1 precipitation product which was developed to support the Global Precipitation Climatology Project (GPCP) established by the World Climate Research Programme to quantify multi-year global distributions of precipitation. The product provides 1-day (daily) precipitation estimates on a 1-degree grid over the entire globe for the period October 1996 - present. The GPCP-1DD product is a complement to the GPCP Version 2 Satellite-Gauge (SG) combination product (Adler et al. 2003). GPCP-1DD uses data from geostationary-satellite infrared sensors to compute the threshold-matched precipitation index (TMPI) and provide precipitation estimates on a 1°×1° grid at 3-hourly intervals within the 40°N–40°S latitude zone. The TMPI sequence of instantaneous 3-hourly estimates are summed to produce the daily value. Estimates outside this latitude zone (not used in this study) are computed based on recalibrated Television Infrared Observation Satellite Operational Vertical Sounder data from polar-orbiting satellites (Susskind et al. 1997). Additionally, the GPCP-1DD product is scaled in both data regions to match the monthly accumulation provided by the SG product which combines satellite and gauge observations at a monthly time scale on a 2.5°×2.5° grid.

3. Analysis method

The analysis method is fairly straightforward and is based on compositing the precipitation data as a function of weather state. The D1.WS.ET.dat file contains the weather state index in each 2.5° grid cell for every daytime 3-hour interval. Due to their different temporal and spatial resolutions the two precipitation data sets have to be treated differently in the compositing process. The 3-hour resolution of the TMPA-3B42 data allows temporal matching with the ISCCP weather state data. Spatial matching to the 2.5° resolution ISCCP weather state data is achieved by taking the mean of all non-missing 0.25° precipitation data that fall into the 2.5° grid cell. GPCP data are resampled from 1° to 2.5° via spatial interpolation.

For each 3-hour time period, the TMPA-3B42 data are segregated for each weather state in order to calculate the state's precipitation statistics. However, something analogous cannot be performed for the daily-averaged GPCP-1DD precipitation data. We therefore pursue two avenues for segregating and compositing GPCP-1DD data: (1) we assign the same daily precipitation rate to all weather states encountered during the daytime period of a grid cell; or (b) we only consider those grid cells for which a single weather state persists during a day's daylight hours and assign the corresponding GPCP-1DD daily precipitation rate (cf. Rossow et al. 2011).

Considering the above, only TMPA-3B42 composited precipitation can be characterized as actual daytime (i.e. during sunlit hours) precipitation. Because the temporal matching with the ISCCP weather states can be performed better, most of our analysis relies on TMPA-3B42 precipitation data. The availability of GPCP-1DD precipitation rates, even without the temporal resolution of TMPA-3B42, may however still offer insight on certain aspects of weather state precipitation, as we will show below. To construct two precipitation composites that are more comparable, we also segregate TMPA-3B42 precipitation as in method (2) of GPCP-1DD compositing, i.e., we consider the daily-averaged TMPA-3B42 precipitation rates of only those grid cells where a single weather state persists during daytime.

As will be seen in the next section, precipitation data that have been segregated by weather state can be analyzed in terms of their range and variability, geographical distributions, relative contributions to the precipitation budget, and other features.

4. Characteristics of tropical weather state precipitation

In this section we identify the relative importance of the various weather states to the tropical precipitation budget, examine the degree to which the weather states are hydrologically distinct, investigate whether a weather state's precipitation is affected by the state that temporally adjoins it, examine the sensitivity of the results to the precipitation dataset used, and perform a separate more detailed analysis on the seasonal and geographical precipitation characteristics of WS1, the most convectively intense weather state.

a. Means and geographic distribution of TMPA-3B42 precipitation

The geographic distribution of the 10-yr mean daytime precipitation rate for each weather state from TMPA-3B42 is shown in Fig. 3. These are mean rates (including zero precipitation) at the time of weather state occurence. It is immediately obvious that ISCCP joint histogram clustering succeeds in isolating the most intensively precipitating weather state, WS1, with its large portion of high optically thick clouds (Fig. 1). WS1's mean precipitation rate indeed dwarfs the precipitation of any other weather state in the tropics with vast regions of the tropical Pacific and Atlantic oceans exhibiting mean annual precipitation rates in excess of 25 mm/day. There are significant regional differences in WS1 precipitation, like smaller rates over the Indian Ocean and weaker precipitation over land (further discussed further). The mean precipitation rates for the remaining weather states generally decrease monotonically with their assigned index, with WS2 and WS3 producing significant precipitation (albeit always lower than 10 mm/day on an annual basis) consistent with their implied level of convective activity (convective anvils that often evolve from WS1 convection in the case of WS2, and unorganized less penetrative convection in the case of WS3). From the convectively suppressed states WS4 to WS8 (grouped together in the precipitation frequency histograms of Rossow et al. 2011), WS8 is notable for a stronger precipitation presence over land areas.

To gauge the hydrological importance of a weather state in the tropics, the contribution of the weather state to the total precipitation of the entire region is calculated. These results are shown in Fig. 4, as percentage contributions of each weather state to the total grid cell precipitation. Two important points need to be kept in mind for the interpretation of these figures. First, the contribution of each weather state to the total grid cell precipitation is not only a function of the mean precipitation intensity when the state occurs, but also of its frequency of occurrence in the particular grid cell. If for example, one compares the top panel of Fig. 3 with the top panel of Fig. 4 (WS1) there is not much spatial correlation between mean precipitation rate and contribution. This is because areas where WS1 produces large precipitation are often also areas where WS1 rarely occurs. Second, areas where a particular weather state appears to be contributing significantly are not necessarily areas where that state produces significant precipitation. In other words, the fractional contribution of a state may be large, but with a small total grid cell precipitation, the absolute amounts of precipitation involved are small even for the largest weather state contributor. An example of this is WS3 with small precipitation amount being the largest contributor of precipitation off the west coast of S. America, a generally dry area (Fig. 3).

The domain-average annual daytime mean precipitation and fractional contribution of each weather state to the total tropical precipitation from TMPA-3B42 is shown in Fig. 5. To facilitate the interpretation of the fractional contribution, the domain-average annual RFO is also included in the graph. One can see that despite an RFO of only ~6%, WS1 contributes about half of the total precipitation of the ±35° latitude zone. This is because the mean precipitation rate of ~19 mm/day for this state is more than four times higher than the next strongest precipitating weather state (WS2). But WS2, as well as WS3, are still significant precipitation contributors, collectively contributing about 34% of the tropical precipitation, i.e., about 67% of the precipitation that does not come from WS1. The most frequent state, WS8, with an RFO ~38% contributes less than 8% to the tropical precipitation budget because of its 2nd smallest (after WS7) mean precipitation rate of ~0.6 mm/day.

Fig. 6 breaks down the results of Fig. 5 into land and ocean domain averages. A 2.5° grid cell is defined as "land" when is contains less than 25% water, "ocean" when it is more that 75% water and "mixed" in all other cases. According to this convention, in our latitude zone 23.1% of 2.5° grid cells are land, 71.4% are ocean, and the remaining 5.5% are "mixed". One striking, and somewhat unexpected finding is that the mean precipitation rate of WS1 is significantly higher over ocean (21 mm/day) than over land (14 mm/day). This basic result was reproduced when GPCP-1DD data is used in place of TMPA-3B42 (not shown). The finding seems to contradict conventional wisdom about the greater vigor (i.e., stronger updrafts) of continental deep convection compared to oceanic deep convection. One possible explanation is the drier environment of continental convection causing the evaporation of a significant fraction of the precipitation before it reaches the ground. This phenomenon, discussed by Geerts and Dejene (2005), who found radar reflectivity profiles peaking at high altitude and decreasing toward the ground in Africa, would be captured by the TMPA-3B42 and GPCP-1DD datasets because of the surface gauge rescaling employed. Another possible mechanism for less precipitation reaching the surface over land could be rain being swept in greater amounts out of the convective cores by the stronger updrafts of continental WS1 systems.

Fig. 6 also shows that while the ranking of the weather states with respect to their contribution to the total precipitation is not different between ocean and land, the relative importance of the different weather states as contributors to the precipitation budget exhibits some changes compared to the overall values. One can see, for example, that WS1 is a larger fractional contributor to ocean precipitation than land precipitation, that the opposite is true for WS8, and that WS2 and WS3 are more on par in ocean precipitation contribution than in land precipitation contribution. Differences in the relative fractional contribution between land and ocean can come from the combination of changes in mean precipitation intensity and RFO. For WS1 we see that the RFO over ocean and land is about the same (0.062 and 0.065, respectively) and the main factor making WS1 a larger relative contributor over ocean is mean WS1 precipitation being greater in marine grid cells. In the case of WS3, where both the mean precipitation and the RFO are substantially different between land and ocean, but in opposite directions, it appears that the greater RFO over land dominates the fractional contribution.

b. Comparisons between different datasets and compositing approaches

We now examine whether global values of mean precipitation and contribution are similar when daily-averaged GPCP precipitation is composited. Because of the different temporal resolution of the GPCP dataset, additional assumptions have to be employed for compositing. The comparison between TMPA-3B42 and GPCP-1DD weather state precipitation is shown in Fig. 7. The top left panel of this figure is the same as in Fig. 5, which shows the domain-average daytime mean and contribution to the total precipitation from our "best" compositing method of TMPA-3B42 data that are temporally matched with ISCCP weather state data. The other panels show results using the alternate compositing approaches discussed in section 3, necessitated by the daily-average nature of the GPCP-1DD data set. The upper right panel shows domain average values obtained by assuming that the GPCP-1DD precipitation is constant throughout the day: all weather states identified during the sunlit period of a grid cell are assigned the same value of precipitation, the (spatially interpolated to 2.5°) diurnal average provided by GPCP-1DD. The lower left panel shows values obtained using only those grid cells for which the same weather state persists during the day's daylight hours. Presumably, for the grid cells satisfying the single weather state condition, the assumption of constant precipitation rate throughout the entire daytime period is better. Note that because close the International Date Line daylight hours may be split between two UTC days containing GPCP-1DD data, this area is under-represented in this form of conditional compositing. In the lower right panel the TMPA-3B42 are composited the same way, i.e., using the daily-averaged TMPA-3B42 precipitation and only those grid cells with occurences of only one weather state during the entire daytime period.

The RFOs are comparable between the two panels that use all weather state data (upper row panels) and the two panels that use only the fraction of grid cells with the same persistent weather state throughout the day (lower row panels). The RFOs of the lower row panels increase relative to those of the upper row panels for the states that have the largest fractions of grid cells with a persistent daytime weather state. This is most notable for WS8 which has an RFO of

0.383 when all the grid cells are accounted for, and an RFO of 0.528 when we only consider the grid cells with no diurnal variability of weather state occurrence. Indeed, for WS8 the fraction of grid cells of the latter type is 18.4%, larger than the counterpart fraction of any other weather state. On the other hand, the RFO of (weakly precipitating) WS7 drops from ~0.085 to 0.039 when implementing this screening because only 6.3% of grid cells (lowest of all weather states) containing WS7 maintain this weather state for the entire daytime period; in other words, WS7 rarely persists during the daytime in the tropics. Overall, the fraction of grid cells with a single weather state during daytime is about 13%, i.e., about 87% of data are discarded to produce the lower two panels of Fig. 7.

Contrasting the upper two panels reveals that using the GPCP-1DD data and the constant daytime precipitation assumption leads to a notably different, but not surprising, picture on the precipitation intensity and relative importance of the three most convective states, compared to TMPA-3B42. The precipitation rate of WS1 falls from ~19 mm/day to ~14.5 mm/day and the fractional contribution from 0.49 to 0.33. On the flip side, the mean precipitation rate and fractional contribution of WS2 and WS3 increase: the ratio of WS2 and WS1 fractional contributions increases from 0.32 for TMPA-3B42 to 0.60 for GPCP-1DD, while the ratio of WS3 to WS1 fractional contributions increases from 0.38 to 0.68. It appears therefore that when WS2 or WS3 are observed in a grid cell on the same day as WS1, the constant daytime precipitation assumption assigns to WS2 and WS3 day-averaged precipitation estimates inflated by the occurrence of WS1 in the hours before or after (this is further examined later). One can of course view this misassignment of precipitation also from the WS1 perspective, with weaker precipitation assigned to WS1 in grid cells where convectively weaker states have also occurred in the same day. Such misassignments seems to be also "benefiting" the convectively suppressed states WS4 to WS8, making them appear somewhat stronger precipitation producers and contributors according to GPCP-1DD compared to TMPA-3B42.

As pointed out earlier, one can attempt to bring the two precipitation data sets on a more equal footing by including in the compositing only the grid cells with a single weather state during daytime. The results from this analysis are shown in the lower two panels of Fig. 7. The domain-average annual precipitation rates and fractional contributions from the two satellite data sets look in this case more similar when partitioned by ISCCP weather state. Some differences remain, such as the different relative contribution strengths of WS2 and WS3 which are closer in GPCP-1DD than TMPA-3B42, but the most important aspect of the analysis, WS1's dominance, has now been restored in GPCP-1DD to the same level as in TMPA-3B42.

The above analysis confirms the significant daytime variations in tropical precipitation indicated by previous studies (e.g., Nesbitt and Zipser 2003). These variations can significantly affect the outcome of compositing a daily-averaged product like GPCP-1DD.

c. Distributions of precipitation within weather states

So far we have been examining only the mean annual precipitation of the ISCCP weather states either on a domain-average or regional scale. With the aid of cumulative precipitation rate histograms we will now look into the distribution of precipitation rates in order to gain better understanding on the range and variability of a state's precipitation. Rossow et al. (2011) discuss in detail other ways of constructing conditional precipitation histograms and their dependence on spatial gridding.

Four sets of cumulative histograms are shown in Fig. 8, where each panel corresponds to the same data set and compositing assumptions as in Fig. 7. The cumulative frequencies are normalized relative to the number of each state's RFO. The first bin is considered non-precipitating and includes all precipitation values below 0.048 mm/day, the lowest precipitating value in the original spatial resolution TMPA-3B42 dataset.

Once again, the upper left panel, based on TMPA-3B42 corresponds to the best possible temporal matching between weather state identification and precipitation. The first, perhaps surprising, feature seen in this panel is that even for the strongest precipitating state, WS1, about half the time WS1 is not precipitating according to TMPA-3B42. The frequent occurrence of non-precipitating WS1 cloud systems reminds us that the ISCCP weather states are only statistical descriptions of cloud regimes that encompass a substantial variety of cloud mixtures. These mixtures may include clouds with significantly higher and lower than WS1 centroid average cloud top pressures and optical depths respectively, that are still more closely related to the WS1 cluster centroid than any of the other centroids. A cursory analysis with one year of ISCCP D1 data indicated that the average cloud top pressure and cloud optical thickness of grid cells containing WS1 was 317 hPa and 10.6 when TMPA-3B42 indicated no precipitation and 291 hPa and 13.5 when precipitation was detected. This finding suggests significant height and extinction differences between non-precipitating and precipitating WS1's. Variability among tropical WS1 has also been implied in the results shown in Fig. 6 of Oreopoulos and Rossow (2011) showing very wide WS1 shortwave and longwave cloud radiative effect histograms. Finally, some zero precipitation WS1 occurences may be due to space and time mis-matches: TRMM obtains an instantaneous sample within a 3-hour period and so does ISCCP, but they do not necessarily coincide within that time interval time, with separations high as 1-2 hours possible. Likewise, because the ISCCP data is spatially sampled at 30 km, and TRMM may not be looking at the same pixels, different areas within the same grid cell may be captured by the two datasets.

The fraction of non-precipitating WS1 occurences drops dramatically when daily-averaged precipitation values are used (the other three panels). This indicates that when WS1 appears in a grid cell at some point during daytime it is highly unlikely that no precipitation will be recorded at some other time during the same day. Indeed, regardless of what data set or assumption is used for compositing daily precipitation, there is never a higher than 10% chance that a grid cell containing WS1 will remain precipitation-free for the entire day.

The frequency of non-precipitating cloud mixtures increases rapidly as one progressively moves to the most convectively suppressed weather states. For example, even for WS3, 86% of occurences are not associated with any precipitation according to TMPA-3B42 (upper left panel). These frequencies are again smaller when daily precipitation averages are composited: the other three panels agree that only ~45% of grid cells containing WS3 at some point during daytime will maintain zero precipitation throughout the day.

At the high end of the precipitation distribution we note from the upper left panel of Fig. 8 that while about 26% of WS1 occurences are associated with rain rates above 24 mm/day, the corresponding percentage drops to about 7% for WS2, 4% for WS3 and more rapidly therafter to values below 0.5% for WS5 to WS8. This part of the histogram changes less by the details of compositing (s result also found by Rossow et al. 2011). For example, the upper right panel based on GPCP-1DD has counterpart values for WS1-WS3 of 23%, 7% and 3% indicating that strong precipitation also tends to be persistent. The cumulative histograms of the last four weather states form a group of histogram curves that is clearly distinct from the other weather states, also characterized by well-separated histograms. This reinforces the fact that the ISCCP weather state centroids are good classifiers of the various tropical precipitation regimes.

d. Precipitation dependence on weather state transitions

Another approach for assessing precipitation variability within weather states is to examine whether a state's precipitation depends on the weather state that precedes or follows it. Intuitively, one would expect some dependence because a particular state's realization may have features that fluctuate according to what preceded or what follows. For example, a cloud mixture classified as WS3 may have differnt features when it follows WS1 instead of (probably more rarely) WS2.

Figure 9 shows the annual-domain averaged precipitation of a weather state as a function of the weather state that either preceded (top panel) or followed (bottom panel). Such an analysis can obviously only be performed with the 3-hourly TMPA-3B42 data set. For all weather states, the mean precipitation rate is stronger when the state is preceded or followed by WS1 (squares enclosed by the red dashed rectangle and the WS1-WS1 square along the diagonal). The frequency with which transitions to or from WS1 happen is, of course, different for each weather state and does not affect the values in the figure which are simply the mean precipitation rates when the state occurs. Interestingly, except for the case it is preceded or followed by itself, WS1 exhibits the strongest precipitation when it is preceded or followed by WS8 than any other weather state, including the ones that are convectively stronger. The transition from WS8 to WS1 and vice-versa is however rare (not shown). One other interesting feature seen in the bottom plot is that the mean precipitation of WS2, WS3 and WS4 falls within the same range of 9-12 mm/day when followed by WS1. This is especially surprising for WS4, which is a rather weakly precipitating state when the analysis is not conditional on close temporal proximity of WS1. But when WS1 precedes, WS2 precipitates more that WS3 and WS4 (top plot). Because of their lower values, the precipitation characteristics of other combinations of weather state transitions (i.e., squares within the black dashed rectangle) do not merit further discussion here. We do, however, show the geographical distribution of the sum of the precipitation values enclosed within the black and red rectangles in the middle panel of Fig. 10. This is simply the map of the mean precipitation rate originating from all weather states except WS1, i.e., WS2 to WS8. This map should be contrasted with the counterpart maps in the top and bottom panels which shows again mean precipitation rates originating from WS2 to WS8, but this time only considering the cases where WS1 either precedes (top panel) or follows (bottom panel), i.e., the same values used for obtaining the means within the red dashed rectangle of Fig. 9. WS2 to WS8 are precipitating stronger everywhere when they are in temporal proximity to WS1, and more so when they precede WS1 rather than follow it. These transition results can be explained by the changing weather states representing different parts of the same storm system. The domain-average precipitation rates for the three panels from top to bottom are 8.16, 1.56 and 10.71 mm/day.

e. Seasonal variations of WS1

Our analysis so far has clearly demonstrated that WS1 is by far the most important weather state for tropical precipitation. This comes as no surprise, since it simply expresses the fact that deep convection is a major contributor of tropical precipitation. In this subsection we perform additional analysis of WS1 precipitation characteristics, focusing on seasonal variations. The seasonal variations of the other states' precipitation were also examined but are not shown because both the precipitation rates and their relative seasonal variability are appreciably weaker. From a domain-average perspective, even the WS1 annual cycle of mean precipitation is not particularly strong (Fig. 11), a result also found by Tselioudis and Rossow (2011). The maximum value occurs in June, but is only ~6% higher than the annual mean; the minimum value occurs in March, but is only ~4.5% below the annual mean. Seasonal variations in the fractional contribution relative to the annual mean are even lower (2.5% above annual mean in October and 2.7% below annual mean in June are the highest deviations). This is because months with relatively high precipitation rates have also relative low RFOs and vice-versa.

Even though the seasonal variations of WS1 domain-average precipitation are not strong, geographical distributions vary significantly with season. The 10-year average seasonal daytime precipitation totals (in mm) of WS1 are shown in the top four panels of Fig. 12. There are substantial zonal movements of WS1 precipitation in accordance with movements of WS1 occurences (shown in the bottom four panels of Fig. 12 as absolute counts). The band of deep convection known as the ITCZ moves northward from DJF to JJA and this is reflected in the northward displacement of WS1 precipitation. WS1 produces the lowest precipitation totals over Africa and S. America in JJA and the highest precipitation totals over south Asia, including India and the bay of Bengal. The eastern equatorial Pacific WS1 precipitation is also stronger during JJA. DJF marks the return of WS1 precipitation south of the equator in Africa and S. America, and is also characterized by high precipitation totals in the South Pacific Convergence Zone and the western part of the maritime continent where WS1 occurence peaks. Thus, while the WS1 precipitation totals of the entire geographical zone do not change by much, the zonal and meridional precipitation movements are quite prominent. Overall, the seasonality of tropical precipitation geographical shifts seems to come primarily from WS1, with other states not exhibiting much geographical motion.

5. Summary and discussion

We provide a comprehensive picture of the relationship between ISCCP weather states (also called cloud regimes by some authors) and precipitation for the entire tropics (35°S to 35°N), thus significantly expanding the limited knowledge from prior studies which were more geographically restricted. Our analysis relies on the concepts of conditional sampling/sorting and composite averaging. By employing these concepts on two widely used merged (satellite and surface) precipitation data sets, TMPA-3B42 and GPCP-1DD we gain insight on how the tropical precipitation budget is partitioned among the various weather states identified by analysis of ISCCP-retrieved cloud properties. We focus primarily on the TMPA-3B42 precipitation dataset because it has the same 3-hour temporal resolution as the ISCCP weather states. Because weather states can only be identified during daytime when cloud optical thickness from passive visible observations is available, our findings, based on 10 years of measurements, only apply to daytime precipitation. GPCP-1DD precipitation compositing applies by nature to diurnally-averaged precipitation.

We find that the mixture of high and optically thick clouds represented by weather state with index "1" (WS1) in the ISCCP data set and considered the most convectively active is associated with almost half the tropical precipitation despite the fact that it occurs only about 6% of the time. This is because its mean precipitation rate at the time of occurrence is about 19 mm/day, more than four times higher than the second most active state (WS2) which happens to also have the second highest mean precipitation rate. The presence of WS1 affects the apparent precipitation of the other weather states: when WS1 occurs in a grid cell before or after another weather state, the precipitation assigned to that state is stronger. It seems therefore that weather states occuring before or after WS1 are affected by its convective progenitors or descendants. But even this weather state appears to be precipitation-free about half the time according to a frequency distribution analysis of TMPA-3B42 precipitation rates. Another feature of WS1 is that it has the strongest seasonal variability of all weather states, still relatively weak on a domain-averaged basis, but with prominent geographical variations. When the precipitation data are composited separately over land and ocean grid cell differences emerge. WS1 precipitates less over land suggesting that updraft strength considerations may be superseded by environmental humidity and its effects on precipitation evaporation. Also, over land the relative contribution of WS3 goes up significantly reaching a value close to half of that of WS1 (over ocean the relative contribution is closer to a quarter of that of WS1).

The choice of the precipitation data set used in the compositing affects the results noticeably. The GPCP-1DD precipitation represents the grid cell diurnal average and cannot be combined with ISCCP weather state data available every 3 hours without further assumptions. When the same daily precipitation rate is assigned to every weather state that may occur within the grid cell during sunlit hours, the contrast between the three most convective weather states is tempered. The domain-average precipitation rates and contributions become much more consistent between the two datasets, as might be expected, when most data are discarded in favor of grid cells with a single weather state persisting during daytime. Apparently, for those cases the GPCP-1DD daily average is a much better representation of the state's precipitation. Diurnally averaged precipitation composites cannot capture as well the frequency of non-precipitating

WS1 occurences, revealing that once WS1 appears in a grid cell it very uncommon that the cell will remain precipitation-free for the entire 24-hour period.

Since clouds are the most prominent regulators of radiation and precipitation, it is natural to explore in future work the connections between precipitation, radiation, and the state of the atmosphere as a function of cloud regime within the weather state framework. Some work along these lines has already been performed to some extent (e.g., Gordon and Norris 2010; Oreopoulos and Rossow 2011; this work), but the unifying effort that will fully integrate the physical relationships between atmospheric dynamical and thermodynamical states and the budgets of radiation and precipitation into a coherent picture has not yet materialized. Once such an effort is completed, a better foundation on how to conjointly analyze cloud regimes and associated meteorology with energy and water budgets will be available for climate models to capitalize on. This can lead to significant leaps in the quality of model hydrology and energetics.

Acknowledgements

Lazaros Oreopoulos and Dongmin Lee acknowledge funding from NASA's Modeling Analysis and Prediction program and the CloudSat/CALIPSO Science Team recompetition, both managed by Dr. David Considine. William B. Rossow acknowledges funding from the NASA MEASURES and NEWS programs. We would like to thank A. Del Genio for helpful discussions.

References

Adler, R. F., and Coauthors, 2003: The Version-2 Global Precipitation Climatology Project (GPCP) Monthly Precipitation Analysis (1979–present). *J. Hydrometeor.*, **4,** 1147–1167.

Geerts, B. and T. Dejene, 2005: Regional and Diurnal Variability of the Vertical Structure of Precipitation Systems in Africa Based on Spaceborne Radar Data. *J. Climate*, **18**, 893–916.

Gordon, N. D. and J. R. Norris, 2010: Cluster analysis of midlatitude oceanic cloud regimes: mean properties and temperature sensitivity. *Atmos. Chem. Phys.*, **10**, 6435-6459.

Greenwald, T. J., Y.-K. Lee, J. A. Otkin, and T. L'Ecuyer, 2010): Evaluation of midlatitude clouds in a large-scale high-resolution simulation using CloudSat observations. *J. Geophys. Res.*, **115**, D19203, doi:10.1029/2009JD013552.

Haynes, J. M., C. Jakob, W. B. Rossow, G. Tselioudis, and J. Brown (2011), Major characteristics of Southern Ocean cloud regimes and their effects on the energy budget, *J. Climate*, in press.

Huffman, G. J., R. F. Adler, M. Morrissey, D. T. Bolvin, S. Curtis, R. Joyce, B McGavock, J. Susskind, 2001: Global Precipitation at One-Degree Daily Resolution from Multi-Satellite Observations. *J. Hydrometeor.*, **2**, 36-50.

Huffman, G. J., R. F. Adler, D. T. Bolvin, E. J. Nelkin, 2010: The TRMM Multi-satellite Precipitation Analysis (TMPA). Chapter 1 in *Satellite Applications for Surface Hydrology*, F. Hossain and M. Gebremichael, Eds. Springer Verlag, ISBN: 978-90-481-2914-0, 3-22.

Jakob, C., and C. Schumacher, 2008: Precipitation and latent heating characteristics of the major Tropical Western Pacific cloud regimes. *J. Climate*, **21**, 4348–4364.

Jakob, C., and G. Tselioudis, 2003: Objective identification of cloud regimes in the Tropical Western Pacific. *Geophys. Res. Lett.*, **30**(21), 2082.

Jakob, C., G. Tselioudis, and T. Hume, 2005: The radiative, cloud, and thermodynamic properties of the major tropical Western Pacific cloud regimes. *J. Climate*, **8**, 1203-1215.

Mekonnen, A. and W.B. Rossow, 2011: The interaction between deep convection and easterly waves over Tropical North Africa: A Weather State perspective. *J. Climate*, **24**, 4276-4294.

Nesbitt, S. W., and E. J. Zipser, 2003: The Diurnal Cycle of Rainfall and Convective Intensity according to Three Years of TRMM Measurements. *J. Climate*, **16**, 1456–1475.

Oreopoulos, L. and W. B. Rossow, 2011: The cloud radiative effects of International Satellite Cloud Climatology Project weather states. *J. Geophys. Res.*, **116**, D12202, doi:10.1029/2010JD015472.

Rossow, W. B. and R. A. Schiffer, 1999: Advances in understanding clouds from ISCCP. *Bull. Amer. Meteorol. Soc.,* **80**, 2261-2288.

Rossow, W.B., G. Tselioudis, A. Polak, and C. Jakob, 2005: Tropical climate described as a distribution of weather states indicated by distinct mesoscale cloud property mixtures. *Geophys. Res. Lett.*, **32**, L21812.

Rossow, W. B., A. Mekonnen, C. Pearl, and W. Goncalves, 2011: Tropical precipitation extremes. *J. Climate*, submitted.

Susskind, J., P. Piraino, L. Rokke, T. Iredell, and A. Mehta, 1997: Characteristics of the TOVS Pathfinder Path A dataset. *Bull. Amer. Meteor. Soc.*, **78,** 1449–1472.

Schiffer, R.A., and W.B. Rossow, 1983: The International Satellite Cloud Climatology Project (ISCCP): The first project of the World Climate Research Programme. *Bull. Amer. Meteor. Soc.*,

64, 779-784.

Tromeur, E. and W. B. Rossow, 2010: Interaction of Tropical Deep Convection with the Large-Scale Circulation in the MJO. *J. Climate*, **23**, 1837–1853.

Tselioudis, G., and W. B. Rossow, 2011: Time scales of variability of the tropical atmosphere derived from cloud-defined weather states. *J. Climate*, **24**, 602-608.

Williams, K. D., and M. J. Webb, 2008: A quantitative performance assessment of cloud regimes in climate models. *Clim. Dyn.,* **33**, 141-157.

Zhang, Y., S. Klein, G. G. Mace, and J. Boyle, 2007: Cluster analysis of tropical clouds using CloudSat data. *Geophys. Res. Lett.*, **34**, L12813, doi:10.1029/2007GL029336.

Zhang, Y., S. A. Klein, J. Boyle, and G. G. Mace, 2010: Evaluation of tropical cloud and precipitation statistics of Community Atmosphere Model version 3 using CloudSat and CALIPSO data. *J. Geophys. Res.*, **115**, D12205, doi:10.1029/2009JD012006.

Figure Captions

Figure 1. Cluster centroids for the 8 weather states of the extended tropics geographical zone (35° S to 35° N) derived from ISCCP D1 data. Each plot shows the normalized frequency of occurrence (in %) within p_c- τ bins.

Figure 2. The geographical distribution of the relative frequency of occurrence (RFO) of the 8 weather states of the extended tropics geographical zone for the period 1998-2007. Values are normalized relative to the total number of weather state occurrences with valid TMPA-3B42 precipitation measurements within the geographical area for this period.

Figure 3. Geographical distribution of the 10-yr mean precipitation rate (mm/day) for each of the 8 extended tropics weather states.

Figure 4. Geographical distribution of the fractional contribution to the total 10-yr grid cell precipitation rate of each weather state.

Figure 5. Domain-average values of the mean precipitation rates and fractional contributions shown in Figs. 3 and 4. Also included is the domain-average RFO of each weather state.

Figure 6. As in Fig. 5, but when TMPA-3B42 precipitation is aggregated separately over ocean (left) and over land (right).

Figure 7. (upper left panel): As in Fig. 5; (upper right panel): as the upper left panel, but using GPCP-1DD precipitation rates, assumed constant throughout the day; (lower left panel): as the upper right panel, but using only those grid cells with the same weather state occurring during daytime; (lower right panel): as the upper left panel, but with precipitation diurnally averaged for those grid cells with the same weather state persisting during daytime.

Figure 8. Cumulative histograms of precipitation rate for each weather state for the precipitation datasets and compositing assumptions used in Fig. 7.

Figure 9. Mean TMPA-3B42 precipitation rate of each each weather state (with "0" designating cloud-free 2.5° cells, and grey squares indicating non-existent combinations) at time *T* as a function of either the weather state 3 hours earlier, *T*-3h (top) or 3 hours later, *T*+3h (bottom). The values within the dashed red rectangle of the upper (lower) panel come from the same precipitation data used for the top (bottom) panel of Fig. 10. The black dashed rectangles contain means from precipitation data used in the middle panel of Fig. 10.

Figure 10. (middle): Geographical distribution of mean total (combined) daytime precipitation rate from TMPA-3B42 of weather states 2 to 8; (top): same as the middle panel, but when the weather state occuring three hours earlier is WS1; (bottom): same as the middle panel, but when the weather state occuring three hours later is WS1. The domain average values are 1.56, 8.16, and 10.71 mm/day, respectively. These panels show the geographical distribution of the sum of the means highlighted in the black and red dashed rectangles of Fig. 9, as explained in the caption of that figure.

Figure 11. 10-yr mean annual cycle of WS1 TMPA-3B42 precipitation when present, fractional contribution to domain precipitation, and RFO.

Figure 12. Geographical distribution of the yearly average seasonal precipitation total (in mm) for WS1 (top four panels) and the average number of WS1 occurrences (bottom four panels).

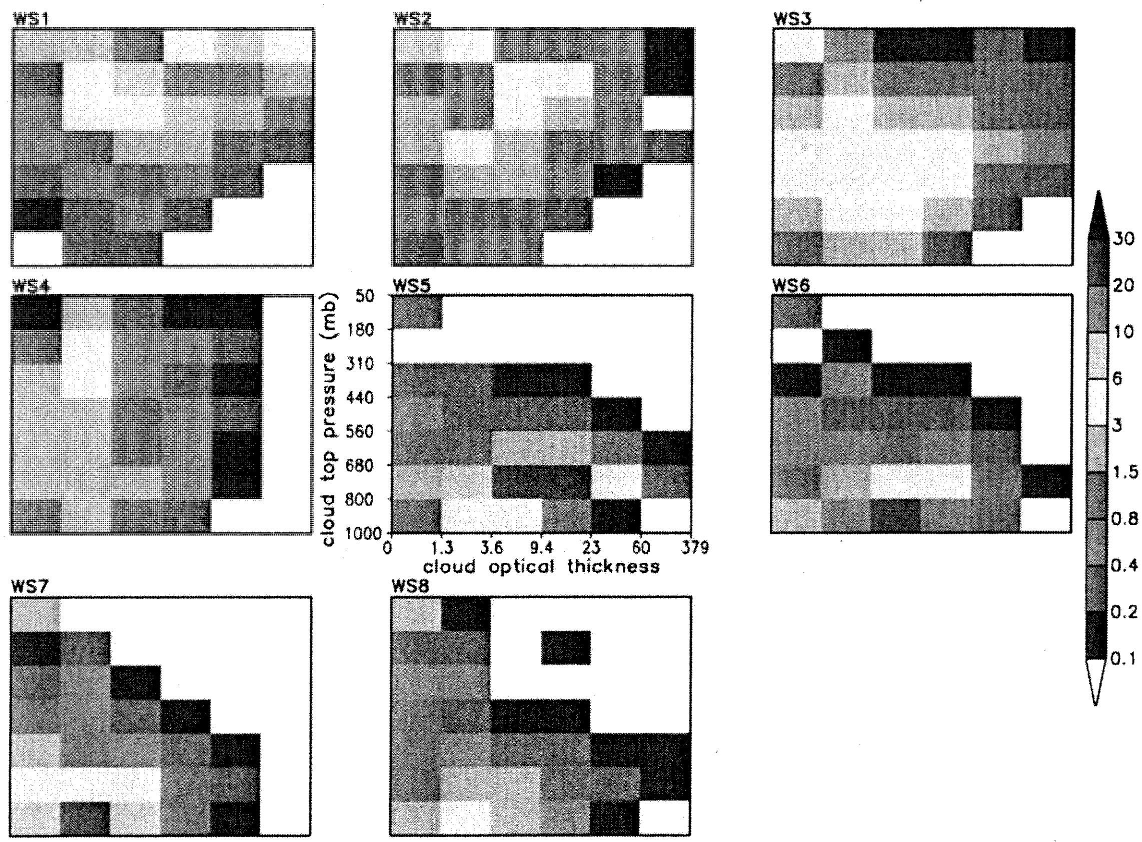
WS1
WS2
WS3
WS4
WS5
WS6
WS7
WS8
cloud top pressure (mb)
50
180
310
440
560
680
800
1000
0
1.3
3.6
9.4
23
60
379
cloud optical thickness
30
20
10
6
3
1.5
0.8
0.4
0.2
0.1

Figure 1

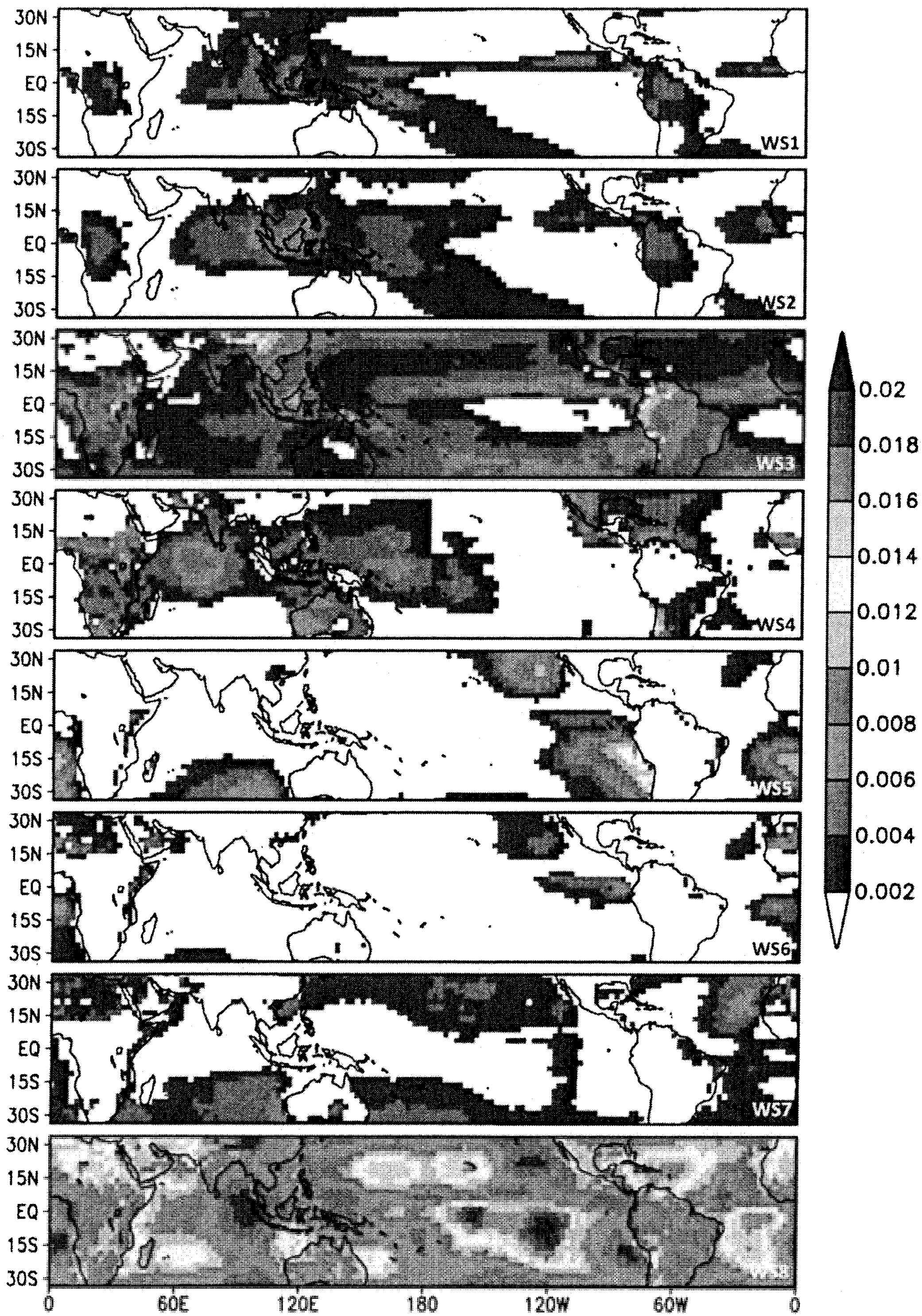
30N
15N
EQ
15S
30S
WS1
WS2
WS3
WS4
WS5
WS6
WS7
WS8
0
60E
120E
180
120W
60W
0
0.02
0.018
0.016
0.014
0.012
0.01
0.008
0.006
0.004
0.002

Figure 2

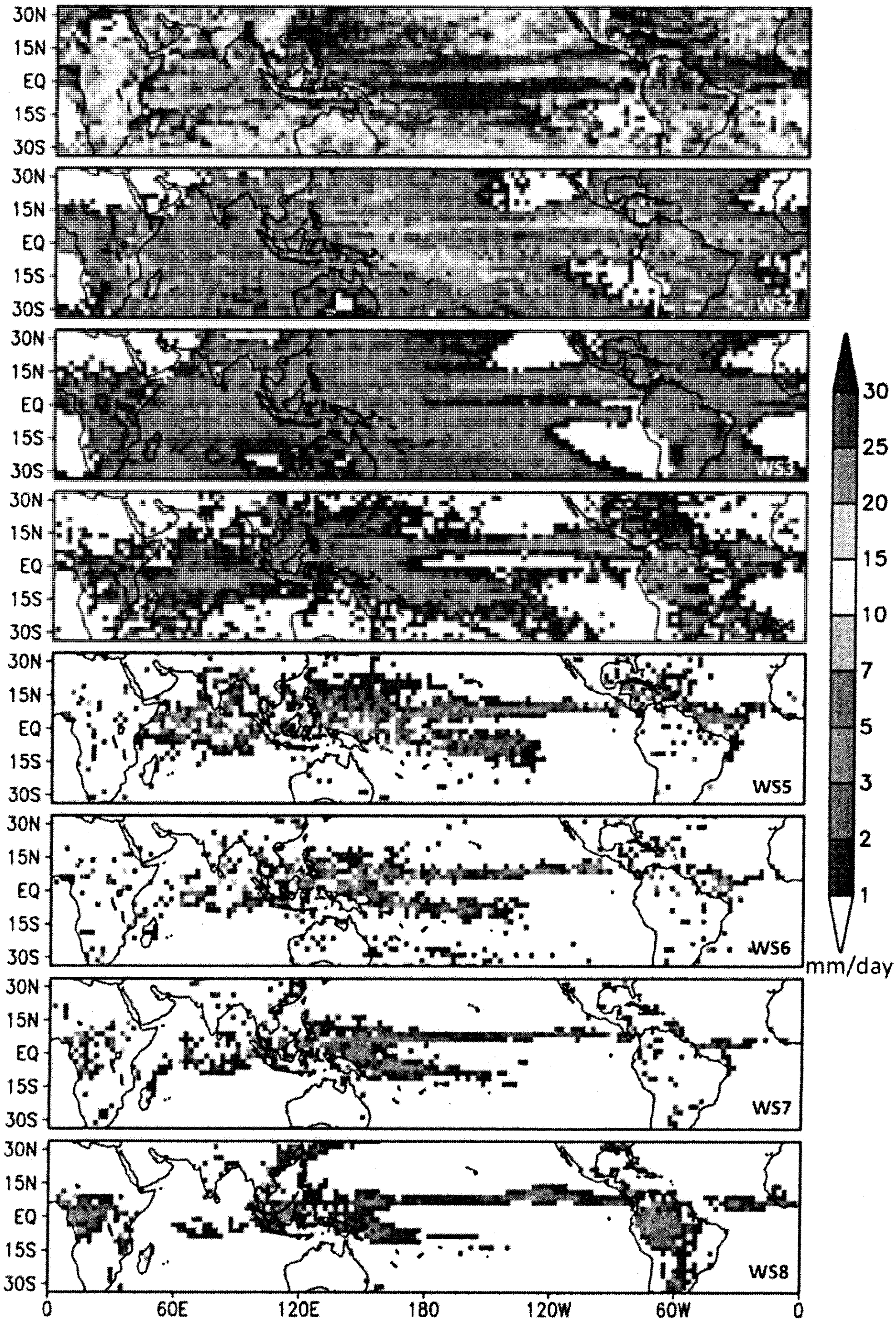
30N
15N
EQ
15S
30S
WS2
WS3
WS4
WS5
WS6
WS7
WS8
0
60E
120E
180
120W
60W
0
30
25
20
15
10
7
5
3
2
1
mm/day

Figure 3

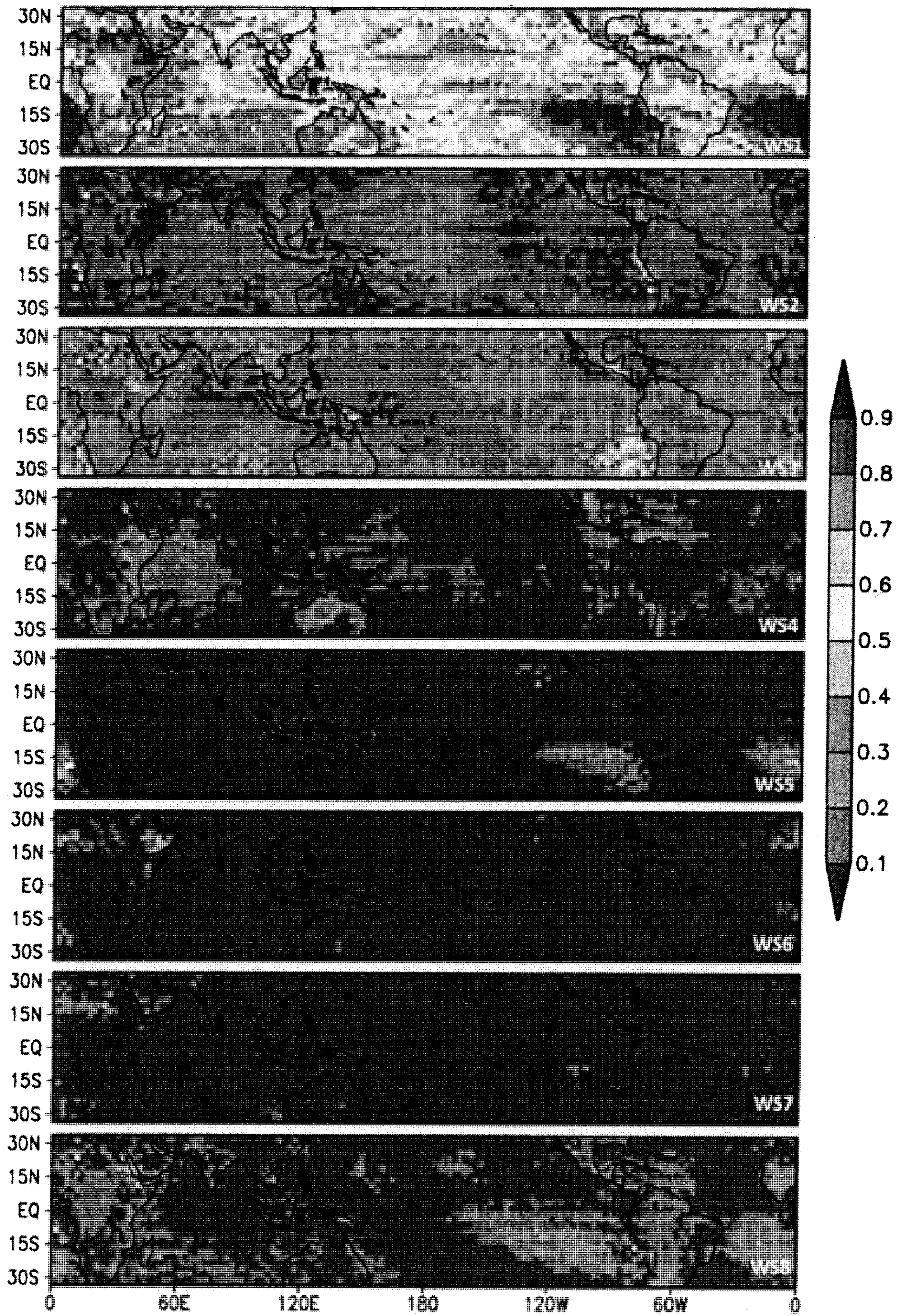
30N
15N
EQ
15S
30S
WS1
WS2
WS3
WS4
WS5
WS6
WS7
WS8
0
60E
120E
180
120W
60W
0
0.9
0.8
0.7
0.6
0.5
0.4
0.3
0.2
0.1

Figure 4

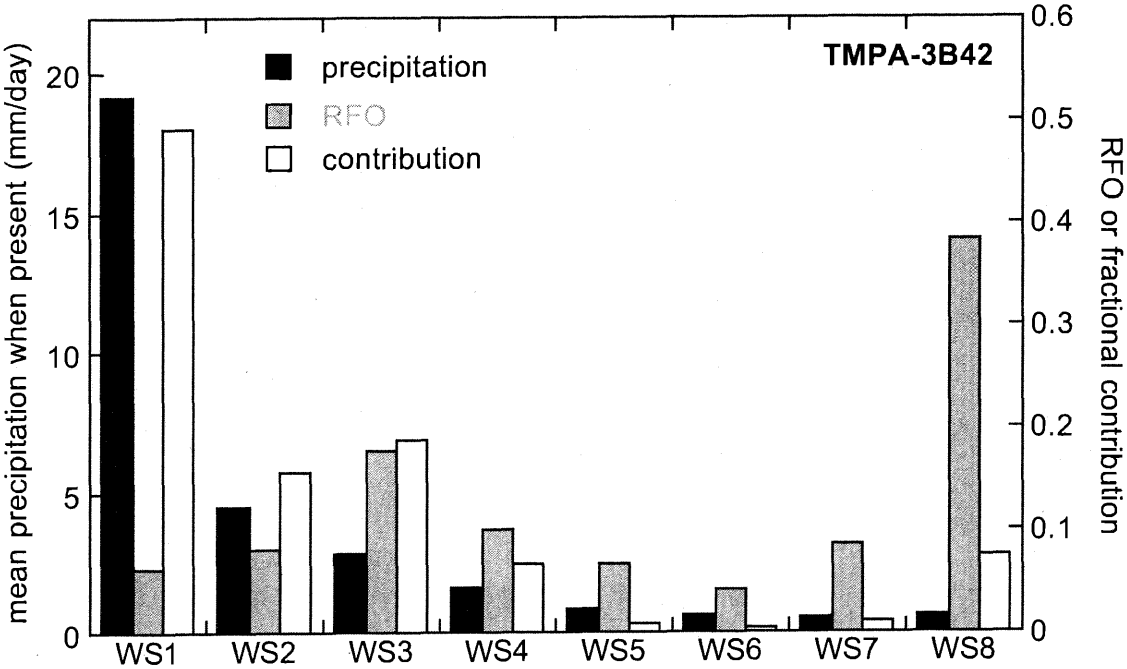
TMPA-3B42
precipitation
RFO
contribution
mean precipitation when present (mm/day)
RFO or fractional contribution
0
5
10
15
20
0
0.1
0.2
0.3
0.4
0.5
0.6
WS1
WS2
WS3
WS4
WS5
WS6
WS7
WS8

Figure 5

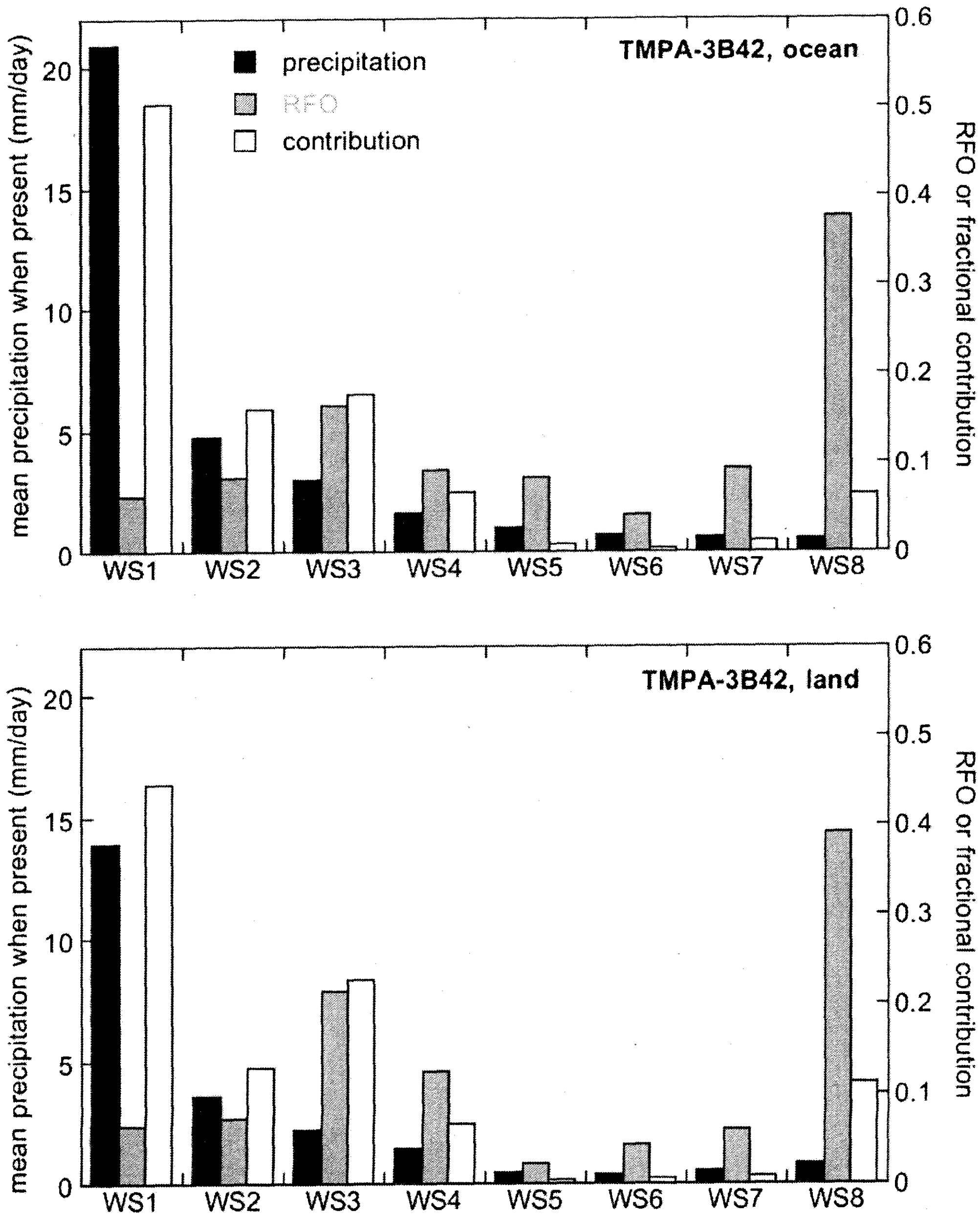
TMPA-3B42, ocean
precipitation
RFO
contribution
mean precipitation when present (mm/day)
RFO or fractional contribution
0
5
10
15
20
0.1
0.2
0.3
0.4
0.5
0.6
WS1
WS2
WS3
WS4
WS5
WS6
WS7
WS8
TMPA-3B42, land
mean precipitation when present (mm/day)
RFO or fractional contribution

Figure 6

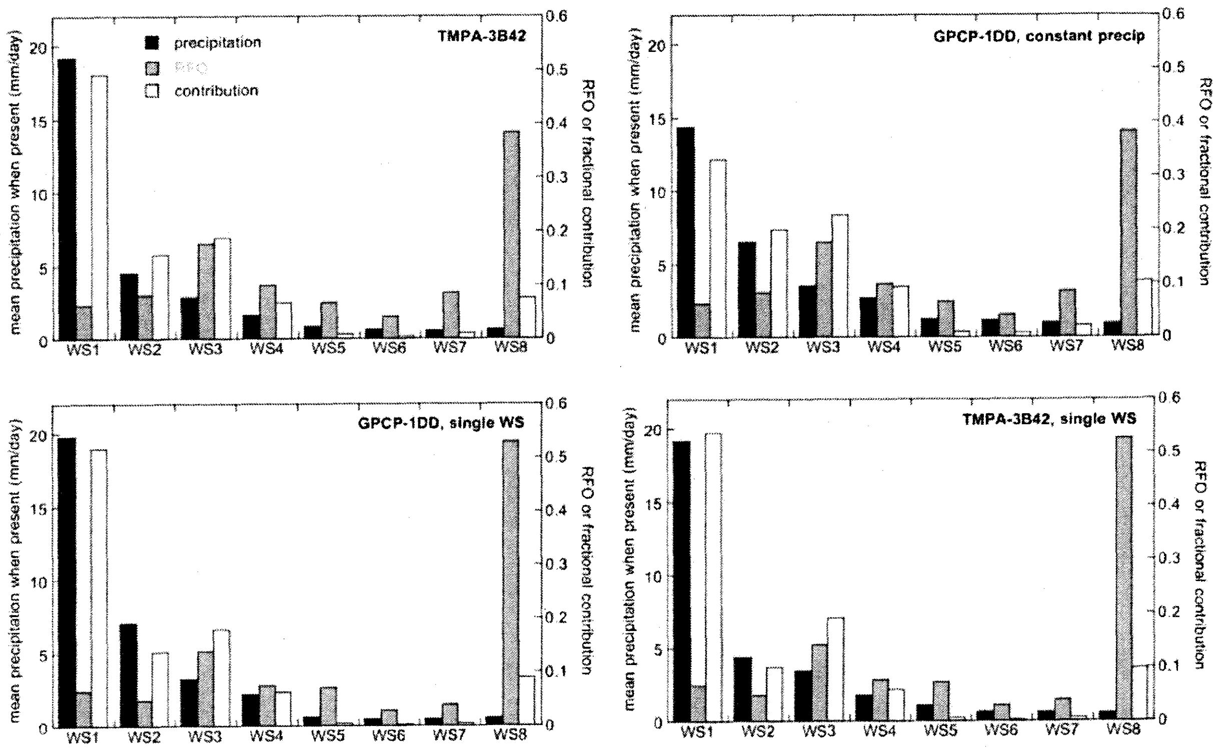
TMPA-3B42
precipitation
RFO
contribution
GPCP-1DD, constant precip
GPCP-1DD, single WS
TMPA-3B42, single WS
mean precipitation when present (mm/day)
RFO or fractional contribution
WS1
WS2
WS3
WS4
WS5
WS6
WS7
WS8

Figure 7

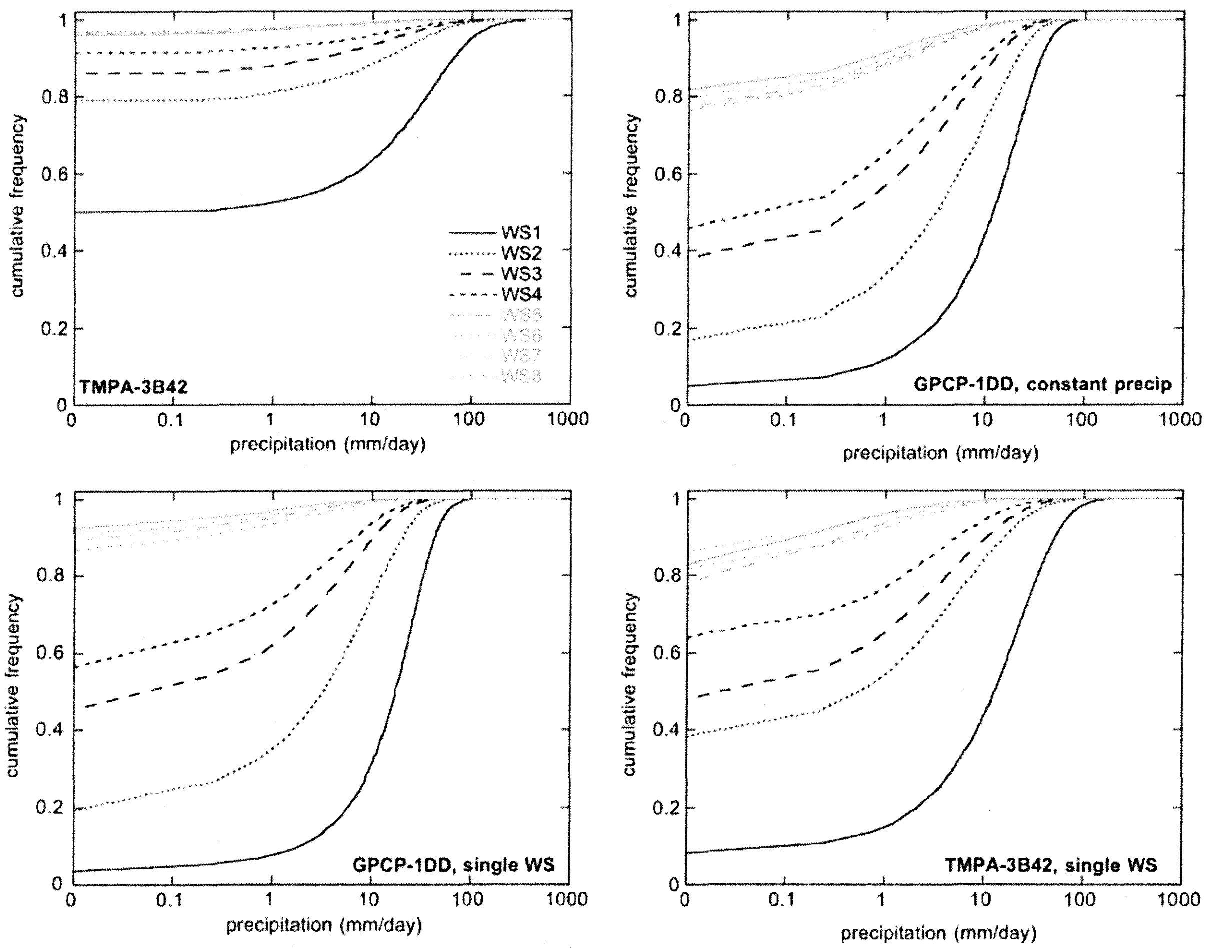
TMPA-3B42
GPCP-1DD, constant precip
GPCP-1DD, single WS
TMPA-3B42, single WS
cumulative frequency
precipitation (mm/day)
WS1
WS2
WS3
WS4
WS5
WS6
WS7
WS8
0
0.1
1
10
100
1000
0.2
0.4
0.6
0.8

Figure 8

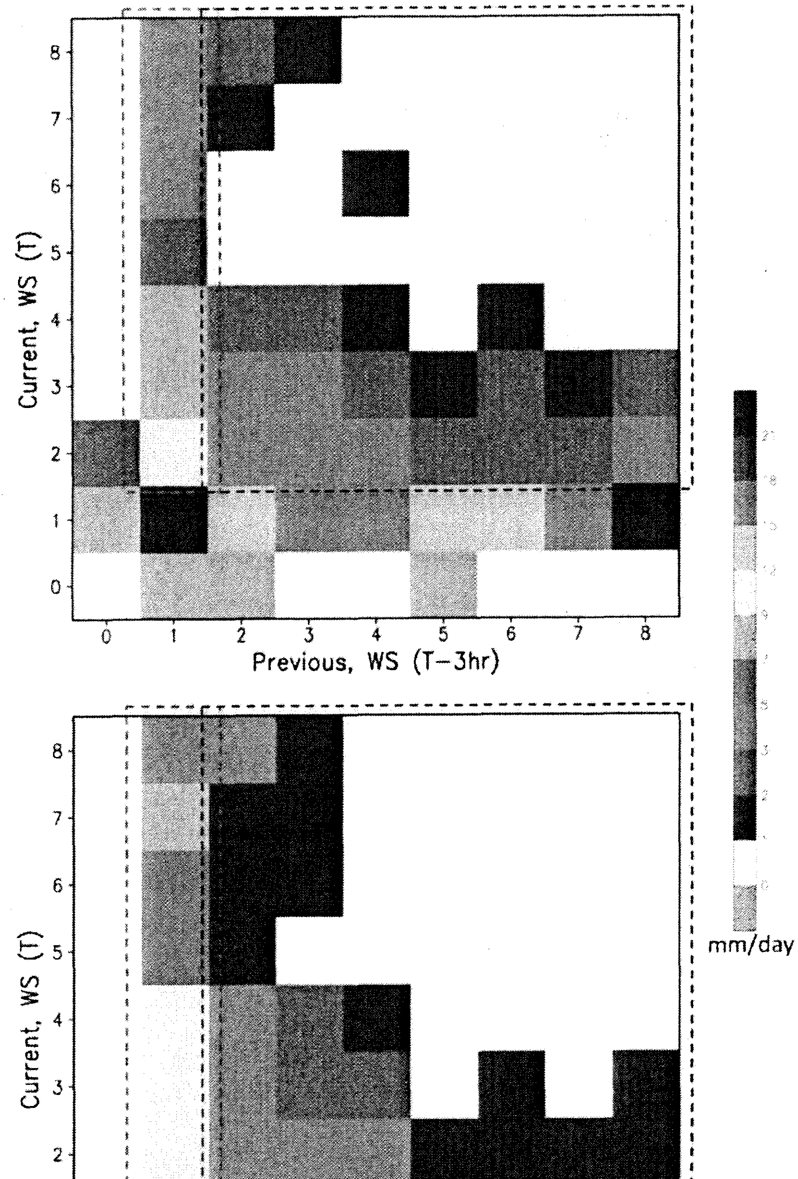

Figure 9

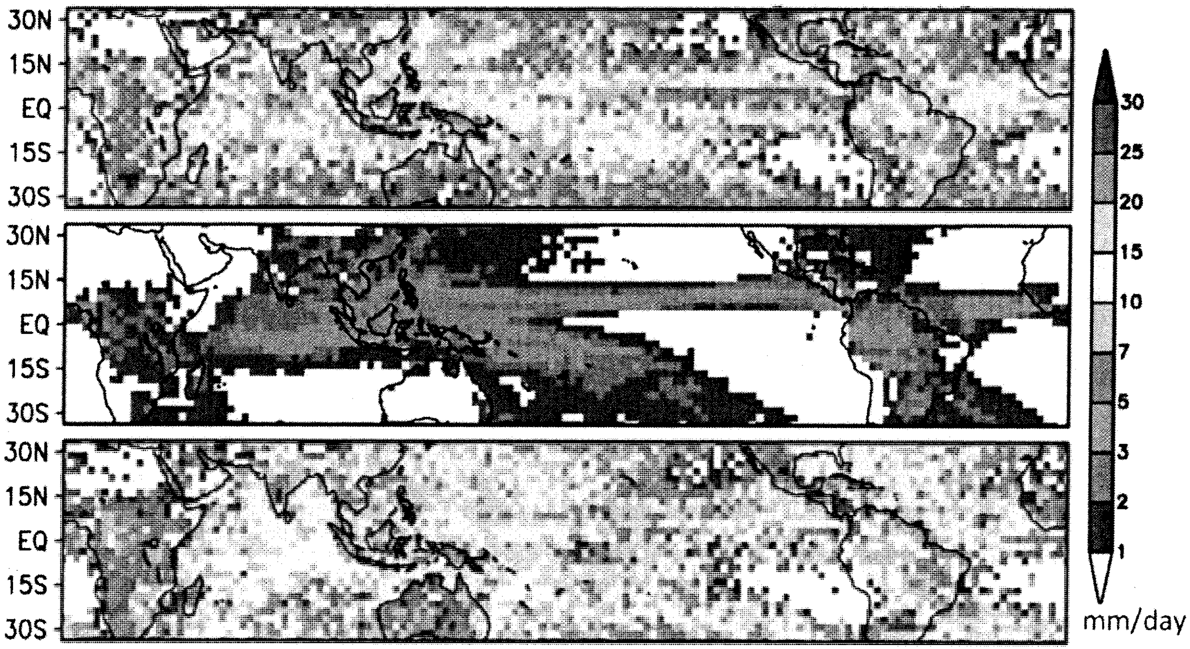

Figure 10

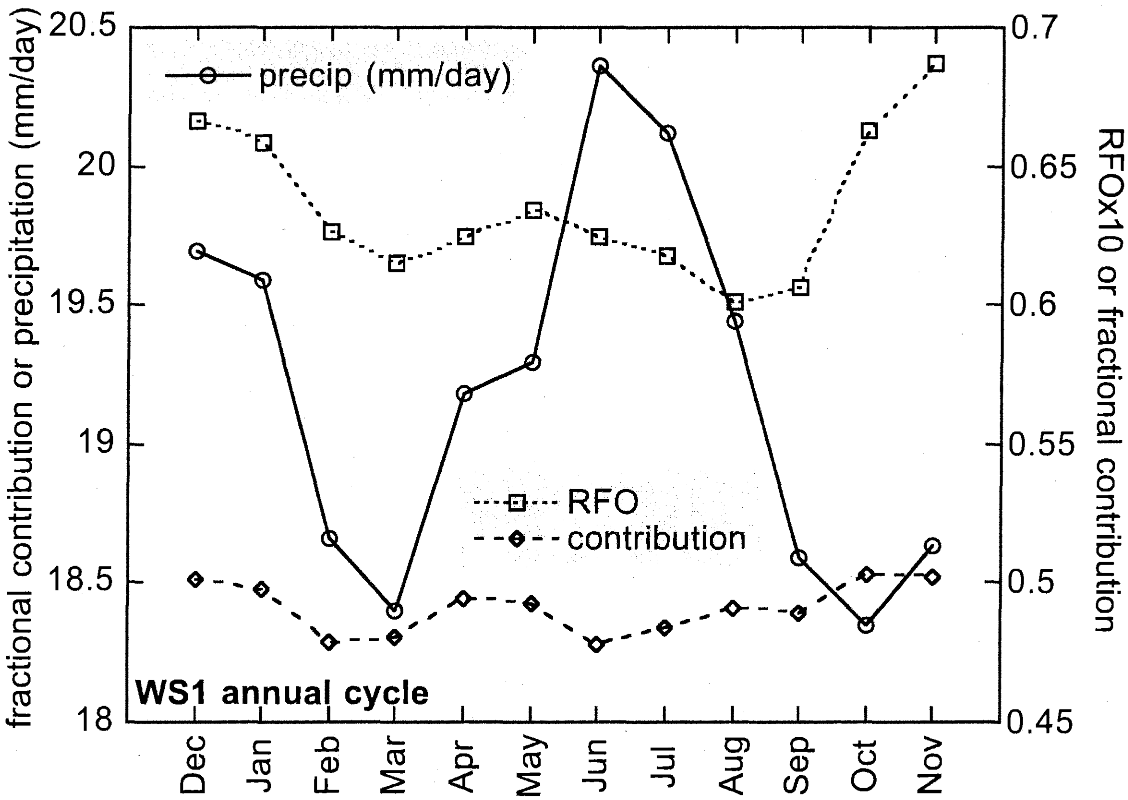

precip (mm/day)
RFO
contribution
WS1 annual cycle
fractional contribution or precipitation (mm/day)
RFOx10 or fractional contribution
20.5
20
19.5
19
18.5
18
0.7
0.65
0.6
0.55
0.5
0.45
Dec
Jan
Feb
Mar
Apr
May
Jun
Jul
Aug
Sep
Oct
Nov

Figure 11

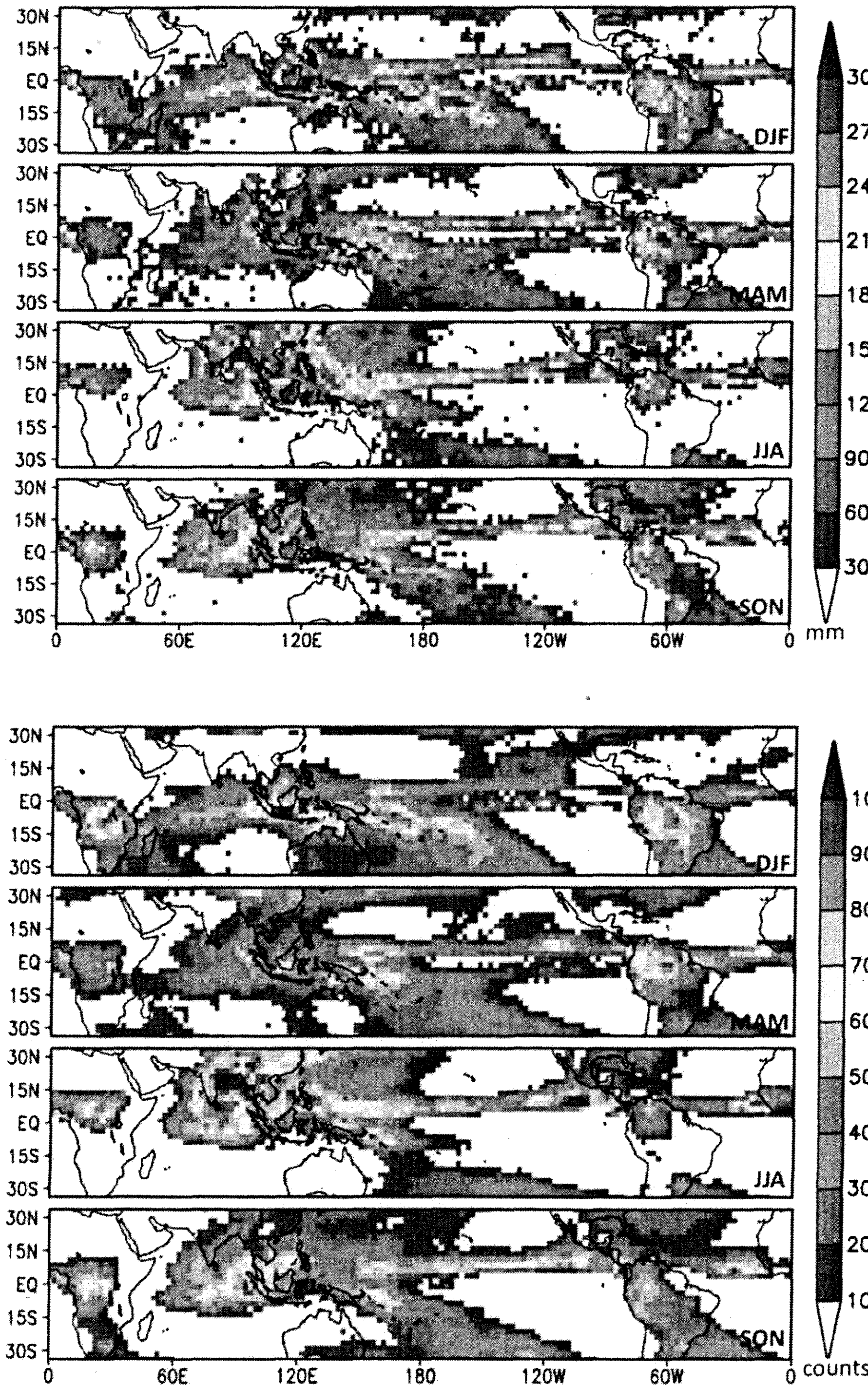
30N
15N
EQ
15S
30S
DJF
MAM
JJA
SON
0
60E
120E
180
120W
60W
0
300
270
240
210
180
150
120
90
60
30
mm
100
90
80
70
60
50
40
30
20
10
counts

Figure 12